computers

MDPI

Article

Performance Analysis of an Adaptive Rate Scheme for QoE-Assured Mobile VR Video Streaming

Thi My Chinh Chu and Hans-Jürgen Zepernick *

Blekinge Institute of Technology, SE-371 79 Karlskrona, Sweden; thi.my.chinh.chu@bth.se
* Correspondence: hans-jurgen.zepernick@bth.se; Tel.: +46-708-78-26-80

Abstract: The emerging 5G mobile networks are essential enablers for mobile virtual reality (VR) video streaming applications assuring high quality of experience (QoE) at the end-user. In addition, mobile edge computing brings computational resources closer to the user equipment (UE), which allows offloading computationally intensive processing. In this paper, we consider a network architecture for mobile VR video streaming applications consisting of a server that holds the VR video content, a mobile edge virtualization with prefetching (MVP) unit that handles the VR video packets, and a head-mounted display along with a buffer, which together serve as the UE. Several modulation and coding schemes with different rates are provided by the MVP unit to adaptively cope with the varying wireless link conditions to the UE and the state of the UE buffer. The UE buffer caches VR video packets as needed to compensate for the adaptive rates. A performance analysis is conducted in terms of blocking probability, throughput, queueing delay, and average packet error rate. To capture the effect of fading severity, the analytical expressions for these performance metrics are derived for Nakagami-*m* fading on the wireless link from the MVP unit to the UE. Numerical results show that the proposed system meets the network requirements needed to assure the QoE levels of different mobile VR video streaming applications.

Keywords: mobile VR; QoE; adaptive rate; prefetching; queueing analysis; performance analysis

Citation: Chu, T.M.C.; Zepernick, H.-J. Performance Analysis of an Adaptive Rate Scheme for QoE-Assured Mobile VR Video Streaming. *Computers* **2022**, *11*, 69. https://doi.org/10.3390/computers11050069

Academic Editor: Chris Headleand, Martin J. Turner and Kai Xu

Received: 9 March 2022
Accepted: 26 April 2022
Published: 29 April 2022

1. Introduction

The tremendous advances in powerful mobile devices and sophisticated communication infrastructure have paved the way to serve the rising demand in a number of high-reliability, high-bandwidth, and low-latency applications. In particular, the rise of mobile immersive media applications such as mobile virtual reality (VR) and mobile augmented reality (AR) put stringent requirements on the performance of emerging 5th-Generation (5G) and anticipated 6G mobile networks in terms of high throughput and ultra-low latency.

Furthermore, it is essential for a successful uptake of these novel applications in a wide range of vertical industries that the user-perceived quality of experience (QoE) is satisfied. As such, network quality assessment has advanced from a pure network operator's quality of service (QoS) focus to also account for the end-user's QoE requirements. The notion of a QoE-aware and QoE-assured design of fixed and mobile networks applies especially to video applications where the end-user is the final judge of quality. Related work includes, e.g., 5G-QoE modeling for ultra-high-definition video streaming in 5G networks [1] and QoE inference from QoS metrics [2].

Given the high computational resources required on mobile devices for media signal processing and the associated strain put on the battery lifetime, modern mobile networks bring enhanced computational power closer to the user equipment (UE) through mobile edge computing (MEC) [3]. As such, MEC-based approaches that allow mobile devices the offloading of computing tasks to the mobile edge play an important role in the delivery of QoE-assured mobile immersive media.

1.1. Related Work

1.1.1. Mobile Edge Computing for VR Videos

In [4], it was forecast that 90% of VR content will be in the form of VR videos, also referred to as 360° videos, omnidirectional videos, surround videos, immersive videos, or spherical videos. Further, better immersive experiences compared to conventional videos can be achieved for VR videos by watching this type of stimuli on a head-mounted display (HMD). Current technologies typically use 4K to 8K resolutions to ensure good visual quality of VR videos when watched on an HMD. Full-view resolutions of 12K and 24K are anticipated to reach an ultimate level of VR QoE in the future, which in combination with frame rates of up to 200 frames per second requires a typical throughput of up to 4.4 Gbps [5]. Given the high throughput and ultra-low latency requirements of this type of VR applications in the context of VR video streaming over the public Internet, new network architectures are needed to assure QoE as the transmission control protocol no longer meets these stringent demands [6]. This applies in particular to network architectures that contain both fixed and mobile networks. The latter induces a time-varying link quality, which in turn would cause contemporary video streaming protocols such as MPEG-DASH to adaptively degrade the video quality with deteriorating transmission conditions [7].

In view of the above challenges, many video QoE improvement techniques have been proposed over the years including video quality adaptation [8–15], prefetching at the UE [16–20], caching at the network edge [21–24], and prefetching at the network edge [25–30].

In [2], a novel mobile edge virtualization with adaptive prefetching system architecture was introduced to achieve QoE-assured 4K video-on-demand delivery. In this system architecture, content intelligence such as caching and prefetching is deployed at the mobile network operator's infrastructure edge. This approach was deployed in a real LTE-A network and assessed for a wide range of realistic network scenarios with applications to 4K video streaming at rates of 15 Mbps and 30 Mbps. It was shown, using an LTE-A C-RAN network testbed infrastructure, that the proposed network architecture always supports seamless playback for video bitrates of up to 30 Mbps and extreme backhaul conditions. Further, practical insights were revealed on the selection of prefetching or other content intelligence for less extreme network conditions to efficiently manage signaling and computing overhead.

A comprehensive survey on mobile augmented reality (MAR) with 5G MEC was provided in [3] covering architectures, applications, and technical aspects. In particular, cloud-based, edge-based, localized, and hybrid architectures for MAR in 5G mobile networks were described, and their advantages and disadvantages were discussed. Among others, for communication applications, it was concluded that MEC-enabled 5G further reduces transport delay because the computational functions are moved closer to the UE. This includes putting network functions to MEC servers using software-defined networking and network functions virtualization, which in turn support more decentralized architectures to better tailor MAR applications. Overall, it is foreseen that the ultra-reliable low-latency communication options offered by 5G mobile networks together with MEC will pave the way for future MAR applications.

The work in [31] proposed a panoramic virtual reality video (PVRV) streaming system for cellular networks using multiconnectivity-based millimeter wave (mmWave) technology in conjunction with MEC to improve the streaming performance in terms of the energy efficiency and quality of the received viewport. While the mmWave links provide the high bandwidth needed by PVRV streaming, a more disruption-free sub-6 GHz link is coupled with those mmWave links that suffer from outages. The task of the MEC server includes finding a tradeoff among link adaptation, transcoding-based chunk quality adaptation, and viewport rendering offloading, which is solved using a fast genetic algorithm. The simulation results show that the PVRV streaming performance offered by the proposed scheme outperforms conventional schemes.

In [32], considering the time-varying nature of wireless channels, a deep reinforcement learning (DRL) approach was used to predict the optimal viewport rendering offloading for MEC-assisted immersive VR video streaming over terahertz (THz) wireless networks. The THz wireless access provides very high data rates and an ultra-reliable link and ensures low delay. The MEC system is used to reduce task-processing latency and the energy consumption that otherwise would be consumed at the HMD. For this purpose, the MEC system performs immersive VR content caching, real-time transcoding, and viewport rendering on behalf of the HMD. An asynchronous-advantage-actor–critic (A3C)-based DLR approach was proposed that optimizes the viewport rendering offloading decision for each immersive VR video chunk and the downlink transmit power of the MEC system. In this way, the long-term average energy consumption of the HMD is minimized. It was shown that the proposed A3C-based DLR algorithm converges fast under different learning rates and outperforms other algorithms in terms of minimizing the energy consumption.

Furthermore, in [33], the long-term QoE of VR users in an MEC-enabled wireless VR network was maximized subject to the VR interaction latency constraint. In particular, a recurrent neural network (RNN) was used to predict the field-of-view (FOV) of each VR user in real-time, while DLR algorithms were used for optimal rendering MEC with model migration from the VR device to the MEC server to maximize the long-term QoE of VR users. The simulation results revealed that the proposed MEC rendering with prediction and migration scheme indeed significantly improves long-term QoE of VR users, as well as VR interaction latency.

In [34], a rendering-aware tile-caching scheme was proposed for 5G MEC networks, which allows multiple cell sites to share their caches in order to optimize the end-to-end latency for VR video delivery in multi-cell MEC networks. The simulation results showed that the proposed rendering-aware VR video-caching scheme achieves superior latency performance compared to systems with decoupled tile caching and rendering.

The work in [35] integrated the digital twin concept into vehicular edge computing (VEC) networks to alleviate the challenges associated with VEC implementation such as the high mobility of vehicles, dynamic vehicular environment, and complex network scheduling. Because digital twins can provide virtual representations of physical networks, it is beneficial to integrate them into VEC networks for predicting, estimating, and analyzing the real-time network state. Similar to the aims of the aforementioned works, an adaptive-digital-twin-enabled VEC network offload problem was solved using a DRL-based offloading scheme to minimize total offloading latency. The simulation results showed that the proposed vehicular offloading algorithm significantly outperforms full offloading to a nearby VEC server and local computing at the vehicles.

A novel unmanned-aerial-vehicle (UAV)-assisted MEC network was proposed in [36] to provide the computing and communication resources required for high-quality mobile 360° video streaming to HMDs. Specifically, the QoE was maximized across all mobile VR users subject to given constraints on the communication resources and the locations of the UAVs. Approximation algorithms were proposed to solve the related NP-hard problem, which turned out to better balance user load compared to two benchmark algorithms.

In [37], a multi-user cost-efficient crowd-assisted delivery and computing (MEC-DC) framework was proposed leveraging MEC and end-user resources to support the high-performance multi-user immersive experience of VR content delivery over 5G heterogeneous networks (5G-HetNets). A buffer evolution model for VR transmissions over 5G-HetNets was proposed to ensure smooth and synchronized user viewing experiences by using stochastic distributed algorithms. The trace-driven experimental results have shown that the proposed solution offers throughput improvements, the lowest delay, and the best playback freeze ratio compared to device-to-device-assisted online reinforcement learning (RL), the RL-based adaptive bitrate solution, and MEC-assisted joint caching and computing.

1.1.2. Quality of Experience

The following definition of QoE was proposed within the COST Action QUALINET and later was also adapted by the International Telecommunication Union (ITU) in Recommendation ITU-T P.10 [38,39]:

"The degree of delight or annoyance of the user of an application or service."

Factors that influence QoE were identified and classified in [40] including human influence factors, system influence factors ranging from media-related factors to network-related factors, and context influence factors. A survey on the evolution of QoE concepts in multimedia systems was given in [41], discussing the ideas behind QoE and providing an overview of related standardization work. QoE metrics for speech, image, and video are also described in this survey. In particular, objective QoE includes measures of the communication process and the task outcome to predict user experience, while subjective QoE measures user experience and user satisfaction through subjective experiments.

In the context of cloud computing, a QoE framework was proposed in [42] with an application to video streaming services. This framework is based on an agent technology and automatically collects objective QoE and QoS measures from the cloud to the client. The framework also provides an option to collect subjective QoE from the users such as complaints and feedback about the services. The work reported in [43] is centered on media-related QoE factors of 360° videos to support the understanding of the impact of video distortions on viewers' visual perception and immersive experiences. A comprehensive review of visual distortions that are induced to 360° videos at the different functions of visual communication processing pipelines was given including optical acquisition, stitching, projection to the code geometry, frame packing, compression, storage and transmission, decompression, frame unpacking, conversion to the display geometry, rendering and viewport extraction, and the HMD. A discussion about measuring 360° video quality was given with respect to subjective metrics, objective metrics, and subjective studies. Recently, in [44], a survey on 360° video was provided covering the most important developments for 360° video coding and compression, subjective and objective QoE, along with the factors that can affect it, salience measurement and viewport prediction, and adaptive streaming of immersive 360° videos. The overview of the research on all the elements of immersive video streaming systems supports the understanding of their interplay and performance.

Concerning the research presented in this paper on QoE-assured mobile VR video streaming, the focus is given to network-related factors such as blocking probability, throughput, queueing delay, and packet error rate (PER). Requirements, challenges, and solutions for this type of cellular-connected wireless VR were discussed in [45]. This work suggests to map the limits of human perception to concrete VR QoS requirements, which the authors referred to as the quality of physical experience. In other words, average human perception values are mapped to QoS requirements with this approach, e.g., the maximum acuity of the human eye is translated to the minimum VR resolution; the area of vision in the human eye corresponds to FOV requirements; the refresh rate in terms of the number of frames per second shown on the HMD is determined by visual acuity and perceived motion continuity. The experience levels introduced in [5] can be seen in light of the above human perception to VR QoS mapping, introducing entry-level VR experiences, advanced VR experiences, and ultimate VR experiences. In this paper, we adopt this classification and consider each of the three experience levels as a distinct QoE class with corresponding QoS requirements.

1.2. Contributions

Motivated by all of the above, in this paper, we conduct a performance analysis of a network architecture for QoE-assured mobile VR video streaming consisting of a server that holds the VR video contents, a mobile virtualization with prefetching (MVP) unit located at the network edge, and an UE comprising of an HMD and a buffer. A wired link is assumed between the server and the MVP unit, while a wireless link is used between the

MVP unit and the UE. The MVP unit performs prefetching of the VR video packets from the server to reduce the latency, which would occur otherwise for VR video contents residing remotely on the public Internet. In addition, the MVP unit offers a number of modulation and coding schemes (MCSs) with different rates, which facilitate adaptive modulation and coding. This adaptive rate scheme copes with the varying channel conditions on the wireless link from the MVP unit to the UE, as well as the state of the buffer at the UE. The buffer at the UE caches the VR video packets requested from the MVP unit as needed to compensate for the induced adaptive rates, which in turn reduces the blocking probability and increases the throughput. A performance analysis of this system was conducted, resulting in analytical expressions for the blocking probability, throughput, delay, and average PER. These performance metrics are derived for the general case of Nakagami-m fading being present on the wireless link between the MVP unit and the UE. This fading model allows capturing and examining the effect of the fading severity on the system performance. Numerical results are provided illustrating that the proposed adaptive rate scheme together with prefetching at the MVP unit and the caching at the UE buffer is able to assure the QoE levels of different mobile VR video streaming applications by controlling the consuming rate and the buffer length at the UE.

The remainder of the paper is organized as follows. In Section 2, the system and channel model, the VR video packet prefetching, and the adaptive rate scheme are described. In Section 3, the queueing analysis of the considered system is provided and the steady-state distribution of the number of packets in the buffer of the UE is derived. In Section 4, the performance of the considered system in terms of blocking probability, throughput, queueing delay, and average PER is analyzed. In Section 5, numerical results are provided, which illustrate the performance of the considered system and its ability to serve different QoE levels (entry-level VR, advanced VR, and ultimate VR). The conclusions are given in Section 6.

2. System Model

Figure 1 shows the system model used for the queueing modeling and performance analysis of the proposed adaptive rate scheme for QoE-assured mobile VR video streaming. It consists of a VR video source acting as the server (content provider) and containing the VR videos, an MVP unit, and mobile UEs. An UE requests VR videos from the VR video source with the help of the MVP unit to run the VR video streaming application. The MVP unit performs prefetching of the VR video packets from the VR video source through a wired network bringing the content closer to the network edge. It also selects the MCS to adapt the rate depending on the wireless channel condition and the state of the buffer at the UE. The buffer at the UE compensates for the varying rates on the wireless channel to essentially maintain the expected rate of the mobile VR video streaming application.

In particular, the transmission from the MVP unit to the UE is divided into time slots of length T_F. The number of packets sent in each transmission depends on the fading condition of the wireless channel and the available positions at the buffer of the UE. The MVP unit provides the requested number of packets, modulates the related bitstream, and then, transmits the resulting signal to the UE. Based on the information about the state of the buffer fed back by the UE to the MVP unit, the number of VR video packets to be prefetched by the MVP unit from the VR video source is chosen such that the maximum number of packets possible to be sent to the UE in a transmission interval T_F is always available. At the UE, the received signal is demodulated to reconstruct the respective number of packets. The obtained packets are then placed into a buffer, which can hold a maximum of L packets.

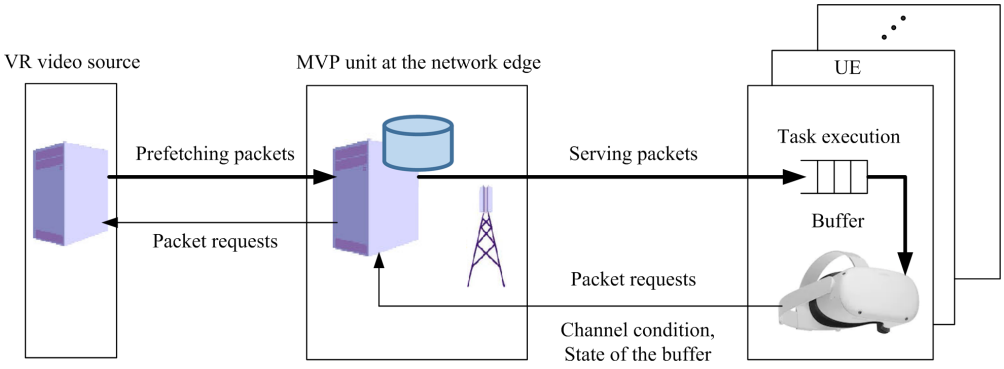

Figure 1. System model of an adaptive rate scheme with prefetching of VR video packets at the MVP unit and caching the packets in a buffer at the UE.

Let the MVP unit select an MCS for each packet based on the condition of the wireless channel, the state of the VR video buffer, and the target PER at the UE. For this purpose, the signal-to-noise ratio (SNR) γ_T at the UE is organized into regions, each of which is associated with a particular MCS, referred to as mode in the following. The switching thresholds defining the minimum SNR needed such that a target PER is maintained by the n-th mode are given by [46]

$$\gamma_n = \frac{1}{g_n} \ln\left(\frac{a_n}{\text{PER}_{TG}}\right), \; n = 1, 2, \ldots, N \tag{1}$$

$$\gamma_{N+1} = \infty \tag{2}$$

where N denotes the number of modes, PER_{TG} is the target PER at the UE, constants a_n and g_n are modulation parameters, and γ_n is the switching threshold for the n-th mode. For example, if $\gamma_T \in [\gamma_n, \gamma_{n+1})$, then the n-th mode is selected. A fitting algorithm was applied in [47] to obtain the constants a_n and g_n. For $N = 5$ modes and $\text{PER}_{TG} = 10^{-3}$, Table 1 shows the five different combinations of binary phase shift keying (BPSK) modulation, quadrature phase shift keying (QPSK) modulation, and 16-ary quadrature amplitude modulation (16-QAM) with error control coding schemes of different code rates. Because the rate in bits per second (bps) of the n-th mode is equal to or greater than n times the rate of Mode 1, we assume that n packets are transmitted during one time slot of length T_F if the n-th mode is selected. Further, we assume that a packet is dropped if it cannot be successfully decoded.

Table 1. Set of modulation and coding schemes and SNR thresholds for a target PER of $\text{PER}_{TG} = 10^{-3}$.

	Mode 1	**Mode 2**	**Mode 3**	**Mode 4**	**Mode 5**
Modulation	BPSK	QPSK	QPSK	16-QAM	16-QAM
Code Rate	1/2	1/2	3/4	9/16	3/4
Rate (bps)	0.50	1.00	1.50	2.25	3.00
a_n	274.72	90.25	67.61	50.12	53.39
g_n	7.99	3.49	1.68	0.66	0.37
γ_n (dB)	1.9518	5.1447	8.2085	12.1477	14.6864

The SNR γ_T at the UE is obtained as

$$\gamma_T = \beta X \;\text{ with }\; \beta = \frac{P}{N_0} \tag{3}$$

where X is the channel power gain of the wireless link from the MVP unit to the UE, β denotes the so-called transmit SNR, P is the transmit power of the MVP unit, and N_0 denotes

the noise power. For a Nakagami-m fading channel with average channel power gain Ω and fading severity parameter m, the probability density function (PDF) and cumulative distribution function (CDF) of the channel power gain X, respectively, are given by

$$f_X(x) = \frac{\alpha^m}{\Gamma(m)} x^{m-1} \exp(-\alpha x) \tag{4}$$

$$F_X(x) = 1 - \exp(-\alpha x) \sum_{i=0}^{m-1} \frac{\alpha^i x^i}{i!} \tag{5}$$

where $\alpha = m/\Omega$. From (3), (4), and (5), the PDF and CDF of the SNR at the UE are obtained as

$$f_{\gamma_T}(\gamma) = \frac{1}{\beta} \frac{\alpha^m}{\Gamma(m)} \left(\frac{\gamma}{\beta}\right)^{m-1} \exp\left(-\frac{\alpha}{\beta}\gamma\right) \tag{6}$$

$$F_{\gamma_T}(\gamma) = 1 - \sum_{i=0}^{m-1} \frac{\alpha^i \gamma^i}{i! \beta^i} \exp\left(-\frac{\alpha\gamma}{\beta}\right) \tag{7}$$

Let the SNR γ_T at the UE be in the range $\gamma_n \leq \gamma_T < \gamma_{n+1}$. Furthermore, assume that the unoccupied positions in the buffer at the UE are q. Then, the v-th MCS mode is selected for the transmission from the MVP unit to the UE as

$$v = \min(n, q) \tag{8}$$

As such, the MCS mode selected for a transmission interval depends on both the channel condition and the state of the buffer at the UE.

3. Queueing Analysis

Let the UE serve a VR video streaming application with processing rate λ, which is equivalent to the average number of packets consumed by the UE in a time slot of duration T_F. In the considered system, the packets served by the UE during the fixed interval T_F occur with a given constant rate λ and independently within this time slot. In this case, the Poisson distribution can be used to express the probability that a given number of packets occurs in a fixed interval.

First, let $p_{k,i}^{(1)}$ denote the probability of the UE consuming k packets of its buffer given that $0 \leq i \leq L$ packets reside in the buffer of length L. Then, the probability $p_{k,i}^{(1)}$ is given as

$$p_{k,i}^{(1)} = \begin{cases} \frac{\lambda^k \exp(-\lambda)}{k!} & \text{for} \quad k \leq i \\ 0 & \text{for} \quad k > i \end{cases} \tag{9}$$

Second, let $p_{h,q}^{(2)}$ denote the probability that h new decoded packets are placed into the buffer conditioned that q empty positions are available in the buffer at the UE. Then, the probability $p_{h,q}^{(2)}$ can be formulated as

$$p_{h,q}^{(2)} = \begin{cases} \sum_{v=h}^{\min(N,q)} p_{h,v,q}^{(3)} & \text{for} \quad h \leq q \\ 0 & \text{for} \quad h > q \end{cases} \tag{10}$$

where the number of modes N also represents the maximum number of packets that the MVP unit can send to the UE in a transmission interval T_F.

Third, let $p_{h,v,q}^{(3)}$ be the joint probability that the MVP unit transmitted v packets and the UE successfully decoded h packets, given q empty positions in the buffer. If $v > q$, then

$p^{(3)}_{h,v,q} = 0$, because the MVP unit knows the buffer state (see Figure 1) and never sends more packets than the number of empty positions in the buffer, as defined in (8). If $v \leq q$ and $v \leq N$, then $p^{(3)}_{h,v,q}$ represents the probability that $\gamma_v \leq \gamma_T \leq \gamma_{v+1}$ and exactly h packets are successfully decoded at the UE. Otherwise, if $v \leq q$ and $v = N$, then $p^{(3)}_{h,v,q}$ is the probability that $\gamma_T \geq \gamma_v$ and exactly h packets are successfully decoded at the UE. In view of the above cases, the joint probability $p^{(3)}_{h,v,q}$ can be expressed as

$$p^{(3)}_{h,v,q} = \begin{cases} \int_{\gamma_v}^{\gamma_{v+1}} s_{h,v}(\gamma) f_{\gamma_T}(\gamma) d\gamma & 0 \leq v < \min(N,q) \text{ and } h \leq v \\ \int_{\gamma_v}^{\infty} s_{h,v}(\gamma) f_{\gamma_T}(\gamma) d\gamma & v = \min(N,q) \text{ and } h \leq v \\ 0 & \text{otherwise} \end{cases} \tag{11}$$

where the probability that exactly h packets of v transmitted packets are decoded is given by

$$s_{h,v}(\gamma) = \binom{v}{h} [1 - P_{e,v}(\gamma)]^h [P_{e,v}(\gamma)]^{v-h} \tag{12}$$

In (12), $P_{e,v}(\gamma)$ is the PER for v packets being transmitted by the MVP unit and an SNR of γ is available at the UE. As in [47], the PER $P_{e,v}(\gamma)$ of the v-th mode can be approximated as

$$P_{e,v}(\gamma) = \begin{cases} 1 & \text{for } 0 < \gamma < \gamma_v \\ a_v \exp(-g_v \gamma) & \text{for } \gamma \geq \gamma_v \end{cases} \tag{13}$$

Then, substituting (13) into (12) and after some algebraic modifications, we obtain

$$s_{h,v}(\gamma) = \begin{cases} 0 & \text{for } 0 < \gamma < \gamma_v \\ \binom{v}{h} \sum_{t=0}^{h} \binom{v}{t} (-1)^t a_v^{t+v-h} \exp(-(t+v-h) g_v \gamma) & \\ & \text{for } \gamma \geq \gamma_v \end{cases} \tag{14}$$

Substituting (6) and (14) into (11) and then applying [48] (Equation (3.381.3)) to solve the resulting integrals, we obtain $p^{(3)}_{h,v,q}$ as in (15). Further, substituting (15) into (10), we obtain the probability $p^{(2)}_{h,q}$ that h new decoded packets are put into the buffer having q empty positions.

$$p^{(3)}_{h,v,q} = \begin{cases} \binom{v}{h} \sum_{t=0}^{h} \binom{h}{t} \frac{(-1)^t \alpha^m a_v^{t+v-h} \left[\Gamma\left(m, \frac{\alpha+\beta(t+v-h)g_v}{\beta} \gamma_v\right) - \Gamma\left(m, \frac{\alpha+\beta(t+v-h)g_v}{\beta} \gamma_{v+1}\right) \right]}{\Gamma(m)(\alpha+\beta(t+v-h)g_v)^m} & \text{for } 0 \leq v < \min(N,q) \text{ and } h \leq v \\ \binom{v}{h} \sum_{t=0}^{h} \binom{h}{t} \frac{(-1)^t \alpha^m a_v^{t+v-h} \Gamma\left(m, \frac{\alpha+\beta(t+v-h)g_v}{\beta} \gamma_v\right)}{\Gamma(m)(\alpha+\beta(t+v-h)g_v)^m} & \text{for } v = \min(N,q) \text{ and } h \leq v \\ 0 & \text{otherwise} \end{cases} \tag{15}$$

Given the expressions of the probabilities $p^{(1)}_{k,i}$, $p^{(2)}_{h,q}$, and $p^{(3)}_{h,v,q}$ in (9), (10), and (15), respectively, the transition probability $\pi_{i,j}$ that the number of packets in the buffer of the UE changes from i in the current transmission interval to j in the subsequent transmission interval can be derived as follows. The transition probability $\pi_{i,j}$ is the joint probability composed of the probability $p^{(1)}_{k,1}$ of the event A that the UE consumes k packets, $0 \leq k \leq \min\{i, N\}$, given i packets are in its buffer, $0 \leq i \leq L$, and the probability $p^{(2)}_{j-i+k,L-i+j}$ of the event B that the UE successfully decodes extra $(j - i + k)$ packets sent from the

MVP unit given $(L - i + k)$ vacant positions in the buffer. Because the events A and B are independent, the transition probability $\pi_{i,j}$ can be calculated as

$$\pi_{i,j} = \sum_{k=0}^{\min\{i,N\}} p_{k,i}^{(1)} p_{j-i+k,L-i+k}^{(2)} \tag{16}$$

Then, substituting the expressions of $p_{k,i}^{(1)}$ given in (9) and $p_{h,q}^{(2)}$ given in (10) into (16) yields

$$\pi_{i,j} = \sum_{k=0}^{\min\{i,N\}} \sum_{v=j-i+k}^{\min(N,L-i+k)} \frac{\lambda^k \exp(-\lambda)}{k!} p_{j-i+k,v,L-i+k}^{(3)} \tag{17}$$

To derive the steady-state distribution of the number of packets in the buffer of the UE, let us define the steady-state probability vector

$$\boldsymbol{\pi} = [\pi_0, \pi_1, \ldots, \pi_L] \tag{18}$$

where π_k, $k = 0, \ldots, L$ denotes the steady-state probability that k packets are in the buffer of the UE. Furthermore, the following conditions apply for the steady-state probabilities:

$$\pi_k \geq 0 \tag{19}$$

$$\sum_{k=0}^{L} \pi_k = 1 \tag{20}$$

In view of (19) and (20), the steady-state probability vector $\boldsymbol{\pi}$ can be obtained as a solution of the system

$$\boldsymbol{\pi}\mathbf{T} = \boldsymbol{\pi} \tag{21}$$

where the transition matrix $\mathbf{T}$ of size $(L+1) \times (L+1)$ contains the transition probabilities $\pi_{i,j}$, i.e.,

$$\mathbf{T} = \left[\pi_{i,j}\right]_{(L+1)\times(L+1)} \tag{22}$$

As can be seen from (21), the steady-state probability vector $\boldsymbol{\pi}$ is a normalized left eigenvector of the transmission matrix $\mathbf{T}$ associated with the eigenvalue one. Utilizing the method of eigenvalue decomposition, which can be performed with the support of mathematical software packages, the left eigenvector of $\mathbf{T}$ corresponding to the eigenvalue one is obtained. Then, we normalize this vector such that all entries sum up to one to obtain $\boldsymbol{\pi}$.

4. Performance Analysis

In this section, we derive analytical expressions for the blocking probability, throughput, queueing delay, and average packet error rate, which allows assessing the performance of the network architecture shown in Figure 1. Nakagami-m fading with fading severity parameter m is used to model the wireless link between the MVP unit and the UE.

4.1. Blocking Probability and Throughput

Blocking probability P_b is defined as the probability that the UE cannot accept packets from the server because the buffer is full. The probability that packets transmitted by the MVP unit are blocked at the buffer of the UE is given by

$$P_b = \pi_L \tag{23}$$

where π_L denotes the steady-state probability that the buffer of length L is fully occupied with packets.

Throughput, also called effective consuming rate, is the rate at which the VR video streaming application of the considered system consumes the packets of the buffer and is calculated as

$$\lambda_T = \lambda(1 - P_b) \tag{24}$$

4.2. Delay in the System and Queueing Delay

The delay induced by an entire system is composed of the transmission delay and the queueing delay, i.e., the time it takes for a packet to be transmitted over a network and the mean waiting time that a packet waits in the buffer until it is processed. The mean waiting time in the buffer at the UE is derived by using the Little's theorem as the ratio between the number of packets in the buffer over the consuming rate. Accordingly, the delay time in the systems is obtained as

$$\delta = \delta_1 + \frac{\sum_{l=0}^{L} l\pi_l}{\lambda} \tag{25}$$

where δ_1 denotes the transmission delay. The numerator in the fraction of (25) represents the long-term average number of packets in the buffer of a stationary system, and the denominator is the consuming rate. It should be mentioned that the transmission delay may be relatively small, e.g., $\delta_1 = 20$ µs in the case of an IEEE 802.11 wireless local area network [49]. In our system model, the prefetching of VR video packets at the MVP unit alleviates the latency related to the public Internet, while the transmission delay from the MVP unit at the network edge to the UE can be assumed as small. Hence, we focus in this work on the queueing delay

$$\delta_2 = \frac{\sum_{l=0}^{L} l\pi_l}{\lambda} \tag{26}$$

4.3. Average Packet Error Rate

The average packet error rate is defined as the ratio of the average number of erroneously decoded packets to the average number of packets transmitted during a transmission interval. In particular, the average number of erroneously decoded packets can be calculated as

$$\overline{\text{PER}} = \frac{1}{\eta} \sum_{n=1}^{N} \overline{\text{PER}}_n \tag{27}$$

where $\overline{\text{PER}}_n$ is the average number of erroneously decoded packets when the n-th MCS mode, $n \leq N$, is selected for the transmission. Furthermore, the average number of packets η transmitted during a transmission interval, also called the average transmission efficiency, can be formulated as

$$\eta = \sum_{n=1}^{N} n p_n \tag{28}$$

where p_n is the probability that the n-th MCS mode is selected, i.e., the probability that n packets are transmitted in a transmission interval. The selection of the n-th MCS mode with $n < N$ takes place for the following two cases:

- **Case 1:** The SNR γ_T at the UE falls in the range $\gamma_n \leq \gamma_T \leq \gamma_{n+1}$, and the buffer has more than n empty positions.

- **Case 2:** The SNR γ_T at the UE falls in the range $\gamma_n \leq \gamma_T$, and the buffer has exactly n empty positions.

Thus, the probability that the n-th MCS mode with $n < N$ is selected for the transmission can be written as

$$p_n = \sum_{i=0}^{L-n-1} \pi_i [F_{\gamma_T}(\gamma_{T_{n+1}}) - F_{\gamma_T}(\gamma_n)] + \pi_{L-n}[1 - F_{\gamma_T}(\gamma_n)] \tag{29}$$

The N-th MCS mode, i.e., highest transmission mode, is selected for the transmission from the MVP unit to the UE if the SNR γ_T at the UE falls in the range $\gamma_N \leq \gamma_T$ and the number of empty positions in the buffer at the UE is greater than or equal to N. The probability of selecting the N-th MCS mode is calculated as

$$p_N = \sum_{i=0}^{L-N} \pi_i [1 - F_{\gamma_T}(\gamma_{T_N})] \tag{30}$$

As such, the total average transmission efficiency combining (29) and (30) is obtained as

$$\eta = \sum_{n=1}^{N-1} n \left[\sum_{i=0}^{L-n-1} \pi_i F_{\gamma_T}(\gamma_{n+1}) - \sum_{i=0}^{L-n} \pi_i F_{\gamma_T}(\gamma_n) + \pi_{L-n} \right] + N \sum_{i=0}^{L-N} \pi_i [1 - F_{\gamma_T}(\gamma_N)] \tag{31}$$

Finally, an expression for the average packet error rate, $\overline{\text{PER}}$, is derived as follows. For $n < N$, the number of erroneous packets for the n-th MCS mode is calculated as

$$\overline{\text{PER}}_n = n \sum_{i=0}^{L-n-1} \pi_i \int_{\gamma_n}^{\gamma_{n+1}} P_{e,n}(\gamma) f_{\gamma_T}(\gamma) d\gamma + n \pi_{L-n} \int_{\gamma_n}^{\infty} P_{e,n}(\gamma) f_{\gamma_T}(\gamma) d\gamma \tag{32}$$

Substituting (6) and (13) into (32) and then applying [48] (Equation (3.381.1)) and [48] (Equation (3.381.4)) to solve the respective integrals, the number of erroneous packets for the case that n packets with $n < N$ are transmitted within a transmission interval is obtained as

$$\overline{\text{PER}}_n = n \sum_{i=0}^{L-n} \pi_i \frac{a_n \alpha^m}{\Gamma(m)} \frac{\Gamma\left(m, \frac{\alpha+\beta g_n}{\beta} \gamma_n\right)}{(\alpha + \beta g_n)^m} + n \sum_{i=0}^{L-n-1} \pi_i \frac{a_{n+1} \alpha^m}{\Gamma(m)} \frac{\Gamma\left(m, \frac{\alpha+\beta g_{n+1}}{\beta} \gamma_{n+1}\right)}{(\alpha + \beta g_{n+1})^m} \tag{33}$$

For $n = N$, the number of erroneous packets for the N-th MCS mode is calculated as

$$\overline{\text{PER}}_N = N \sum_{i=0}^{L-N} \pi_i \int_{\gamma_N}^{\infty} P_{e,n}(\gamma) f_{\gamma_T}(\gamma) \text{d}\gamma \tag{34}$$

Substituting (6) and (13) into (34) and applying [48] (Equation (3.381.1)) to solve the integral, after some algebraic modifications, the number of erroneous packets when N packets are transmitted during one transmission interval is given by

$$\overline{\text{PER}}_N = N \sum_{i=0}^{L-N} \pi_i \frac{\alpha^m a_N}{\Gamma(m)} \frac{\Gamma\left(m, \frac{\alpha+\beta g_N}{\beta} \gamma_N\right)}{(\alpha + \beta g_N)^m} \tag{35}$$

Eventually, substituting (31), (33), and (35) into (27), the average PER is obtained as

$$\overline{\mathrm{PER}} = \frac{\sum_{n=1}^{N-1} n \sum_{i=0}^{L-n-1} \pi_i \frac{a_{n+1}\alpha^m}{\Gamma(m)} \frac{\Gamma\left(m, \frac{\alpha+\beta g_{n+1}}{\beta}\gamma_{n+1}\right)}{(\alpha+\beta g_{n+1})^m} + N \sum_{i=0}^{L-N} \pi_i \frac{a_N \alpha^m}{\Gamma(m)} \frac{\Gamma\left(m, \frac{\alpha+\beta g_N}{\beta}\gamma_N\right)}{(\alpha+\beta g_N)^m}}{\sum_{n=1}^{N-1} n \left(\sum_{i=0}^{L-n-1} \pi_i F_{\gamma_T}(\gamma_{n+1}) - \sum_{i=0}^{L-n} \pi_i F_{\gamma_T}(\gamma_n) + \pi_{L-n} \right) + N \sum_{i=0}^{L-N} \pi_i [1 - F_{\gamma_T}(\gamma_N)]} \tag{36}$$

5. Numerical Results

In this section, we present the numerical results illustrating the performance of the considered adaptive rate scheme with prefetching of VR video packets. To benchmark the performance of the considered scheme, values of key performance indicators (KPIs) as suggested in [5] are provided in Table 2 for different QoE levels (entry-level VR, advanced VR, ultimate VR). In full-view transmission, the data transmitted to the UE contains the full view of the sphere while the bandwidth can be conserved with FOV transmission that transmits high-quality VR video of the current FOV.

The encoded video frames of VR videos are segmented into packets, which, in this work, are assumed to have a size of 1024 bytes. Further, we set the average channel power gain on the wireless link between the MVP unit and the UE to $\Omega = 2$, the fading severity parameter to $m = 2$, and the transmit SNR to $\beta = P/N_0 = 20\,\mathrm{dB}$. In addition, we varied the fading severity parameter as $m = 1, 2, 3$ to study its impact on the throughput.

Table 2. Network requirements in terms of selected key performance indicators (KPIs) of cloud VR for different QoE levels [5].

Weak-Interaction VR Services			
KPI	**Entry-Level VR**	**Advanced VR**	**Ultimate VR**
Typical throughput	Full view: 75 Mbps (2D) 120 Mbps (3D)	Full view: 630 Mbps	Full view: 4.4 Gbps
	FOV: 40 Mbps (2D) 63 Mbps (3D)	FOV: 340 Mbps	FOV: 2.34 Gbps
Typical round-trip time	30 ms (2D) 20 ms (3D)	20 ms	10 ms
Typical packet loss	2.4×10^{-5}	10^{-6}	10^{-6}
Strong-Interaction VR Services			
KPI	**Entry-Level VR**	**Advanced VR**	**Ultimate VR**
Typical throughput	120 Mbps (2D) 200 Mbps (3D)	1.4 Gbps	3.36 Gbps
Typical round-trip time	10 ms	5 ms	5 ms
Typical packet loss	10^{-5}	10^{-6}	10^{-6}

Figure 2 shows the blocking probability P_b as a function of the consuming rate λ for different buffer lengths L. It can be seen that the blocking probability steeply reduces with the consuming rate increasing up to $\lambda = 50$ packets/ms for the considered buffer lengths. For consuming rates $50 < \lambda \leq 450$ packets/ms, the reduction of the blocking probability is less significant. As far as the blocking probability is concerned, instead of relying on high consuming rates to clear the buffer, the increase of the buffer length seems to be more efficient to avoid blocking. In particular, for the consuming rate of $\lambda = 50$ packets/ms and a buffer length of $L = 20$ packets, the blocking probability P_b can be kept below 10^{-8}. Assuming that a blocked packet is lost for further processing in practice, the network

requirements on typical packet loss given in Table 2 are fulfilled for all considered QoE levels and interaction types for the buffer length of 20 packets with consuming rates of $\lambda \geq 50$ packets/ms. For entry-level VR, a buffer length of $L = 15$ packets is already sufficient to achieve the required typical packet loss rate.

Figure 3 presents the throughput λ_T supported by the considered system versus buffer length L for different consuming rates λ. Similar to the blocking probability, the throughput converges to a constant plateau once the buffer length reaches $L = 10$ packets with minor increases obtained for larger buffer lengths. The throughput supported by these consuming rates is given in parenthesis. While an increase of throughput with an increased consuming rate is expected, an increase of the buffer length also improves the throughput. This behavior can be explained with the blocking probability shown in Figure 2, which shows that the larger buffer lengths significantly reduce the blocking probability. As a result, an increased number of packets can be processed, which in turn increases the throughput for a given consuming rate (see also (24)). The results shown in this figure can be used to select the consuming rate needed to fulfill the typical throughput requirements specified in Table 2. For example, given a consuming rate of $\lambda = 450$ packets/ms, all three QoE levels of strong-interaction VR services can be served. The typical throughput requirements of full-view VR, entry-level VR, and advanced VR of weak-interaction and strong-interaction VR services can already be reached with a consuming rate of $\lambda = 175$ packets/ms. As such, Figure 3 may be used to select the buffer length and consuming rate needed to comply with the typical throughput of a particular VR service.

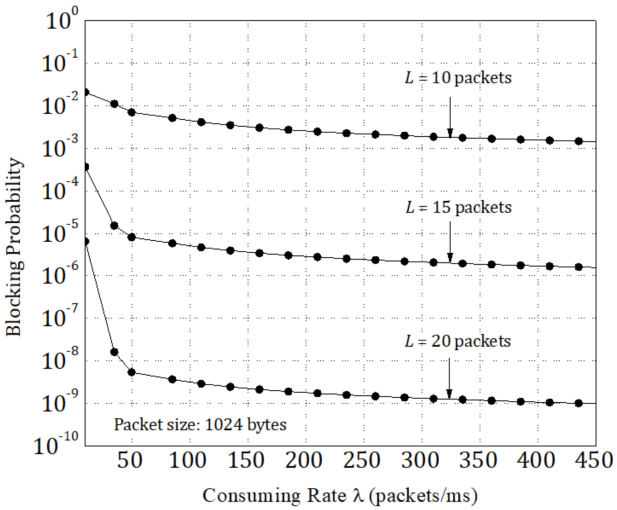

Figure 2. Blocking probability P_b versus consuming rate λ for buffer lengths of $L = 10, 15$, and 20 packets.

Figure 4 shows the delay induced by the queueing system on the overall delay budget of a VR service (see Table 2). The results show that the queueing delay consumes very little of the overall delay budget or typical round-trip time specified in Table 2 to range between 5 ms and 30 ms. In particular, for the buffer length $L \geq 10$ and consuming rate $\lambda = 10$ packets/ms that supports a throughput of $\lambda_T = 81.92$ Mbps, the queueing delay is already kept below 0.6 ms, leaving significant time to be consumed by other functions of the transmission chain. In the case of the increased consuming rate $\lambda = 450$ packets/ms with the associated throughput of $\lambda_T = 3.69$ Gbps, the delay induced by the queueing system is negligible compared to the typical round-trip times allowed to reach the QoE levels of the different interaction types of VR services. In essence, while the increase of the buffer length increases the mean waiting time of a packet in the buffer, an increase of the consuming rate can efficiently compensate for this effect, providing a significant decrease of queueing delay.

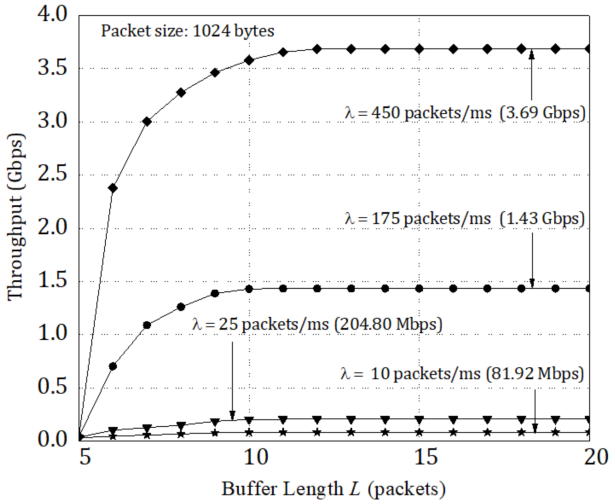

Figure 3. Throughput λ_T versus buffer length L for consuming rates of $\lambda = 10, 25, 175$, and 450 packets/ms.

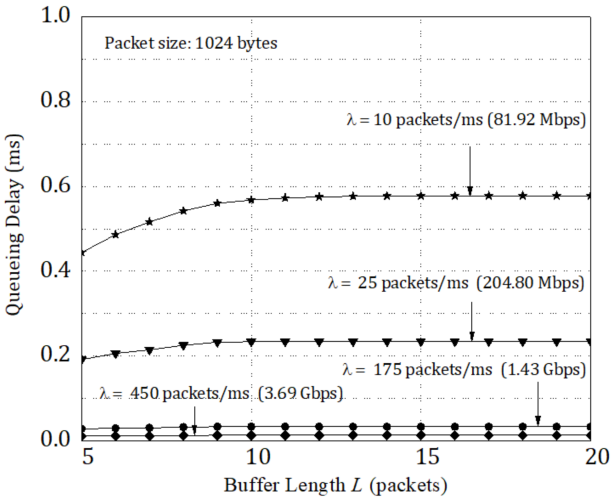

Figure 4. Queueing delay δ_2 versus buffer length L for consuming rates of $\lambda = 10, 25, 175$, and 450 packets/ms.

Figure 5 depicts the average packet error rate, $\overline{\text{PER}}$, as a function of the buffer length L. While the average PER for different consuming rates are fanned out for the smaller buffer lengths from $L = 5$ to 10, a floor of $\overline{\text{PER}} = 4.62 \times 10^{-6}$ is reached for larger buffer lengths. The increase of the average PER with increasing buffer length L is because the MCS mode $n \leq L$ selected at the MVP unit is restricted not only by the wireless channel condition, but also by the number of available unoccupied positions in the buffer. As a result, if the buffer is short, implying a higher risk that only a small number of unoccupied positions can be provided, an MCS mode is selected that uses low-order modulation constellations and low code rates. As the buffer length increases, MCS modes having higher-order modulation constellations and higher code rates can be used, which in turn reduces the robustness against poor wireless channel conditions and increases the average PER. If the buffer length is sufficiently large, the average PER is constrained entirely by the channel condition and converges toward a constant level. The beneficial effect of an increased consuming rate giving a lower average PER may be attributed to the associated increase of the average transmission efficiency (see (28) and (31)) compared to the increase of the MCS-mode-specific average PER (see (27), (29), and (30)).

Figure 6 illustrates the throughput performance of the considered system for different fading severity parameters and consuming rates set to $\lambda = 175$ packets/ms and

$\lambda = 450$ packets/ms. In particular, the fading severity parameter $m = 1$ relates to Rayleigh fading, while the fading severity reduces with increased fading severity parameter $m = 2$ and $m = 3$. For both consuming rates and buffer length $L \leq 10$, throughput becomes higher for less-severe fading channels, i.e., higher fading severity parameter m. An increased buffer length reduces the blocking probability, which results in an increased throughput for all considered fading severity parameters (see also Figure 3 and the related discussion). The throughput becomes independent of the fading severity for buffer length $L > 10$, reaching a constant value of 1.43 Gbps for the consuming rate $\lambda = 175$ packets/ms and 3.69 Gbps for $\lambda = 450$ packets/ms. It should be noted that fading severity may be compensated by beamforming techniques as used in contemporary wireless VR implementations [50,51] and suggested for future wireless local area networks [52].

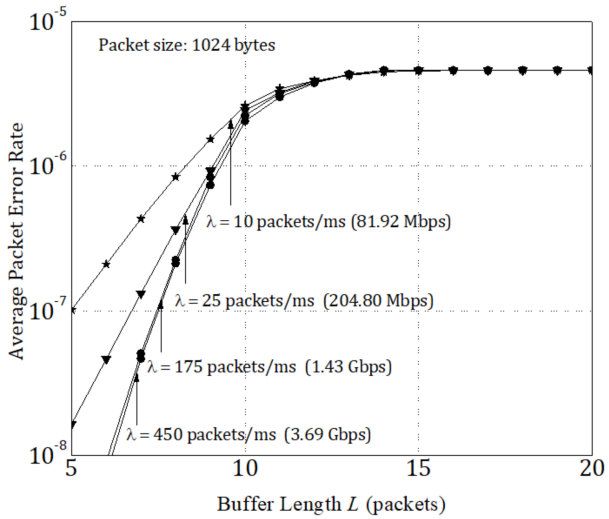

Figure 5. Average packet error rate $\overline{\text{PER}}$ versus buffer length L for consuming rates of $\lambda = 10, 25, 175,$ and 450 packets/ms.

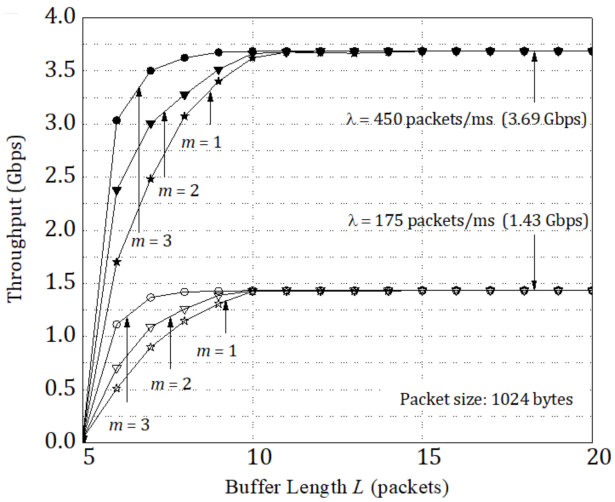

Figure 6. Throughput λ_T versus buffer length L for different fading severity parameter, i.e., $m = 1$ (Rayleigh fading), $m = 2$, and $m = 3$.

6. Conclusions

In this paper, we have conducted a performance analysis of an adaptive rate scheme for QoE-assured mobile VR video streaming. The considered network architecture consists of a server with the VR video contents, an MVP unit at the network edge, and UEs comprising of an HMD and a buffer. The MVP unit prefetches VR video packets from the server, bringing the content closer to the network edge, which reduces the latency. Further, the

MVP unit provides a number of MCS modes for adaptive modulation and coding to cope with the varying conditions of the wireless link to the UE. The selection of the MCS modes and associated adaptive rates is controlled by the channel condition between the MVP unit and the UE, as well as the state of the buffer at the UE. The buffer at the UE compensates for the adaptive rates such that the expected rate of the mobile VR streaming application is maintained, which in turn reduces the blocking probability. The performance analysis has provided analytical expressions for the blocking probability, throughput, queueing delay, and average PER for the general case of Nakagami-*m* fading. Numerical results have been provided illustrating that the adaptive rate scheme together with prefetching at the MVP unit and caching of VR video packets at the UE buffer assures the QoE levels of different mobile VR applications by controlling the consuming rate and the buffer length at the UE.

Author Contributions: Conceptualization, T.M.C.C. and H.-J.Z.; methodology, T.M.C.C. and H.-J.Z.; software, T.M.C.C.; validation, T.M.C.C. and H.-J.Z.; formal analysis, T.M.C.C. and H.-J.Z.; investigation, T.M.C.C. and H.-J.Z.; writing—original draft preparation, T.M.C.C.; writing—review and editing, H.-J.Z.; visualization, T.M.C.C.; supervision, H.-J.Z.; project administration, H.-J.Z.; funding acquisition, H.-J.Z. All authors have read and agreed to the published version of the manuscript.

Funding: This work was supported in part by the Knowledge Foundation, Sweden, through the ViaTecH project under Contract 20170056.

Institutional Review Board Statement: Not applicable.

Informed Consent Statement: Not applicable.

Data Availability Statement: Data is contained within the article.

Conflicts of Interest: The authors declare no conflict of interest.

Abbreviations and Notations

The following abbreviations are used in this manuscript:

16-QAM	16-ary quadrature amplitude modulation
5G	5th-Generation
5G-HetNets	5G heterogeneous networks
6G	6th-Generation
A3C	Advantage actor–critic
AR	Augmented reality
BPSK	Binary phase shift keying
CDF	Cumulative distribution function
C-RAN	Cloud radio access network
DRL	Deep reinforcement learning
FOV	Field of view
HMD	Head-mounted display
KPI	Key performance indicator
LTE-A	Long-term evolution-advanced
MAR	Mobile augmented reality
MCS	Modulation and coding scheme
MEC	Mobile edge computing
MEC-DC	Multi-user cost-efficient crowd-assisted delivery and computing
mmWave	Millimeter wave
MPEG-DASH	Moving Picture Experts Group-dynamic adaptive streaming over HTTP
MVP	Mobile virtualization with prefetching
PDF	Probability density function
PER	Packet error rate
PVRV	Panoramic virtual reality video
QoE	Quality of experience
QoS	Quality of service

QPSK	Quadrature phase shift keying
RL	Reinforcement learning
RNN	Recurrent neural network
SNR	Signal-to-noise ratio
UAV	Unmanned aerial vehicle
UE	User equipment
VEC	Vehicular edge computing
VR	Virtual reality

The following notations are used in this manuscript:

Symbol	Description
$\binom{\cdot}{\cdot}$	Binomial coefficient
$\exp(\cdot)$	Exponential function
$\min(\cdot,\cdot)$	Minimum operator returning the smallest value of two values
a_n	Modulation parameter
$f_X(\cdot)$	Probability density function of random variable X
g_n	Modulation parameter
m	Fading severity parameter
$p_{h,q}^{(2)}$	Probability that h new decoded packets are placed into the buffer conditioned that q empty positions are available in the buffer at the UE
$p_{h,v,q}^{(3)}$	Joint probability that the MVP unit transmitted v packets and the UE successfully decoded h packets given q empty positions in the buffer
$p_{k,i}^{(1)}$	Probability of the UE consuming k packets of its buffer given that $0 \leq i \leq L$ packets reside in the buffer
p_n	Probability that the n-th MCS mode is selected for transmission
$s_{h,v}(\gamma)$	Probability that exactly h packets of v transmitted packets are decoded
$F_X(\cdot)$	Cumulative distribution function of random variable X
L	Length of the buffer at the UE
N	Number of modulation and coding modes
N_0	Noise power
P	Transmit power
P_b	Blocking probability
$P_{e,v}(\gamma)$	Packet error rate for v packets being transmitted by the MVP unit and a signal-to-noise ratio of γ is available at the UE
$\overline{\overline{\text{PER}}}$	Average number of erroneously decoded packets
$\overline{\text{PER}}_n$	Average number of erroneously decoded packets when the n-th MCS mode is selected
PER_{TG}	Target packet error rate
T_F	Duration of a time slot
$\mathbf{T}$	Transition matrix
X	Channel power gain
β	Transmit signal-to-noise ratio
δ	Delay time
δ_1	Transmission delay
δ_2	Queuing delay
η	Average number of packets transmitted during a transmission interval
γ_n	Switching threshold for the n-th MCS mode
γ_T	Signal-to-noise ratio at the UE
λ	Processing rate
λ_T	Throughput
π_k	Steady-state probability that k packets are in the buffer of the UE
$\pi_{i,j}$	Transition probability for the buffer going from state i to state j
$\boldsymbol{\pi}$	Steady-state probability vector
$\Gamma(\cdot)$	Gamma function
$\Gamma(\cdot,\cdot)$	Incomplete gamma function
Ω	Average channel power gain

References

1. Nightingale, J.; Salva-Garcia, P.; Alcaraz Calero, J.M.; Wang, Q. 5G-QoE: QoE Modelling for Ultra-HD Video Steaming in 5G Networks. *IEEE Trans. Broadcast.* **2018**, *64*, 621–634. [CrossRef]
2. Ge, C.; Wang, N.; Foster, G.; Wilson, M. Toward QoE-Assured 4K Video-on-Demand Delivery through Mobile Edge Virtualization with Adaptive Prefetching. *IEEE Trans. Multimed.* **2017**, *19*, 2222–2237. [CrossRef]
3. Siriwardhana, Y.; Porambage, P.; Liyanage, M.; Ylianttila, M. A Survey on Mobile Augmented Reality with 5G Mobile Edge Computing: Architectures, Applications, and Technical Aspects. *IEEE Commun. Surv. Tutor.* **2021**, *23*, 1160–1192. [CrossRef]
4. Huawei iLab. *VR Big Data Report*; Huawei Technologies Co., Ltd.: Shenzhen, China, 2017.
5. Huawei iLab. *Cloud VR Bearer Networks—Huawei iLab VR Technology White Paper*; Huawei Technologies Co., Ltd.: Shenzhen, China, 2017.
6. Ameur, C.B.; Mory, E.; Cousin, B.; Dedu, E. TcpHas: TCP for HTTP Adaptive Streaming. In Proceedings of the IEEE International Conference on Communications, Paris, France, 21–25 May 2017; pp. 1–7.
7. Nagashima, T.; Kanai, K.; Katto, J. QoS and QoE Evaluations of 2K and 4K Video Distribution Using MPEG-DASH. In Proceedings of the IEEE Global Conference on Consumer Electronics, Nagoya, Japan, 24–27 October 2017; pp. 1–2.
8. Akhshabi, S.; Begen, A.C.; Dovrolis, C. An Experimental Evaluation of Rate-Adaptation Algorithms in Adaptive Streaming over HTTP. In Proceedings of the ACM Conference on Multimedia Systems, San Jose, CA, USA, 23–25 February 2011; pp. 157–168.
9. Jiang, J.; Sekar, V.; Zhang, H. Improving Fairness, Efficiency, and Stability in HTTP-based Adaptive Video Streaming with FESTIVE. *IEEE/ACM Trans. Netw.* **2014**, *22*, 326–340. [CrossRef]
10. Mok, R.K.P.; Luo, X.; Chan, E.W.W.; Chang, R.K.C. QDASH: A QoE-Aware DASH System. In Proceedings of the ACM Multimedia Systems Conference, Chapel Hill, NC, USA, 22–24 February 2012; pp. 11–22.
11. Thang, T.C.; Ho, Q.D.; Kang, J.W.; Pham, A.T. Adaptive Streaming of Audiovisual Content Using MPEG DASH. *IEEE Trans. Consum. Electron.* **2012**, *58*, 78–85. [CrossRef]
12. Li, Z.; Zhu, X.; Gahm, J.; Pan, R.; Hu, H.; Begen, A.C.; Oran, D. Probe and Adapt: Rate Adaptation for HTTP Video Streaming at Scale. *IEEE J. Sel. Areas Commun.* **2014**, *32*, 719–733. [CrossRef]
13. Essaili, A.E.; Schroeder, D.; Steinbach, E.; Staehle, D.; Shehada, M. QoE-Based Traffic and Resource Management for Adaptive HTTP Video Delivery in LTE. *IEEE Trans. Circuits Syst. Video Technol.* **2015**, *25*, 988–1001. [CrossRef]
14. Beben, A.; Wiśniewski, P.; Batalla, J.M.; Krawiec, P. ABMA+: Lightweight and Efficient Algorithm for HTTP Adaptive Streaming. In Proceedings of the International Conference on Multimedia Systems, Klagenfurt, Austria, 10–13 May 2016; pp. 2:1–2:11.
15. Zhou, C.; Lin, C.W.; Guo, Z. mDASH: A Markov Decision-Based Rate Adaptation Approach for Dynamic HTTP Streaming. *IEEE Trans. Multimed.* **2016**, *18*, 738–751. [CrossRef]
16. Wang, X.; Kwon, T.; Choi, Y.; Wang, H.; Liu, J. Cloud-Assisted Adaptive Video Streaming and Social-Aware Video Prefetching for Mobile Users. *IEEE Wirel. Commun.* **2013**, *20*, 72–79. [CrossRef]
17. Krishnamoorthi, V.; Carlsson, N.; Eager, D.; Mahanti, A.; Shahmehri, N. Quality-Adaptive Prefetching for Interactive Branched Video Using HTTP-Based Adaptive Streaming. In Proceedings of the ACM International Conference on Multimedia, Orlando, FL, USA, 3–7 November 2014; pp. 317–326.
18. Krishnamoorthi, V.; Carlsson, N.; Eager, D.; Mahanti, A.; Shahmehri, N. Bandwidth-Aware Prefetching for Proactive Multi-Video Preloading and Improved HAS Performance. In Proceedings of the ACM International Conference on Multimedia, Brisbane, Australia, 26–30 October 2015; pp. 551–560.
19. Wilk, S.; Schreiber, D.; Stohr, D.; Effelsberg, W. On the Effectiveness of Video Prefetching Relying on Recommender Systems for Mobile Devices. In Proceedings of the IEEE Annual Consumer Communications & Networking Conference, Las Vegas, NV, USA, 9–12 March 2016; pp. 429–434.
20. Master, N.; Dua, A.; Tsamis, D.; Singh, J.P.; Bambos, N. Adaptive Prefetching in Wireless Computing. *IEEE Trans. Wirel. Commun.* **2016**, *15*, 3296–3310. [CrossRef]
21. Wang, X.; Chen, M.; Taleb, T.; Ksentini, A.; Leung, V.C.M. Cache in the Air: Exploiting Content Caching and Delivery Techniques for 5G Systems. *IEEE Commun. Mag.* **2014**, *52*, 131–139. [CrossRef]
22. Fajardo, J.O.; Taboada, I.; Liberal, F. Improving Content Delivery Efficiency Through Multi-Layer Mobile Edge Adaptation. *IEEE Netw.* **2015**, *29*, 40–46. [CrossRef]
23. Claeys, M.; Bouten, N.; De Vleeschauwer, D.; Van Leekwijck, W.; Latré, S.; De Turck, F. An Announcement-Based Caching Approach for Video-on-Demand Streaming. In Proceedings of the International Conference on Network and Service Management, Barcelona, Spain, 9–13 November 2015; pp. 310–317.
24. Ge, C.; Wang, N.; Skillman, S.; Foster, G.; Cao, Y. QoE-Driven DASH Video Caching and Adaptation at 5G Mobile Edge. In Proceedings of the ACM Conference on Information-Centric Networking, Kyoto, Japan, 26–28 September 2016; pp. 237–242.
25. Chen, S.; Shen, B.; Wee, S.; Zhang, X. Segment-Based Streaming Media Proxy: Modeling and Optimization. *IEEE Trans. Multimed.* **2006**, *8*, 243–256. [CrossRef]
26. Krishnamoorthi, V.; Carlsson, N.; Eager, D.; Mahanti, A.; Shahmehri, N. Helping Hand or Hidden Hurdle: Proxy-Assisted HTTP-Based Adaptive Streaming Performance. In Proceedings of the International Symposium on Modeling, Analysis and Simulation of Computer and Telecommunication Systems, San Francisco, CA, USA, 14–16 August 2013; pp. 182–191.

27. Dong, K.; He, J.; Song, W. QoE-Aware Adaptive Bitrate Video Streaming over Mobile Networks with Caching Proxy. In Proceedings of the International Conference on Computing, Networking and Communications, Garden Grove, CA, USA, 16–19 February 2015; pp. 737–741.
28. Kleinrouweler, J.W.; Cabrero, S.; Cesar, P. Delivering Stable High-Quality Video: An SDN Architecture with DASH Assisting Network Elements. In Proceedings of the ACM International Conference on Multimedia Systems, Klagenfurt, Austria, 10–13 May 2016; pp. 4:1–4:10.
29. Liu, J.; Wan, J.; Jia, D.; Zeng, B.; Li, D.; Hsu, C.H.; Chen, H. High-Efficiency Urban Traffic Management in Context-Aware Computing and 5G Communication. *IEEE Commun. Mag.* **2017**, *55*, 34–40. [CrossRef]
30. Alkassab, N.; Huang, C.T.; Chen, Y.; Choi, B.Y.; Song, S. Benefits and Schemes of Prefetching from Cloud to Fog Networks. In Proceedings of the IEEE International Conference on Cloud Networking, Prague, Czech Republic, 25–27 September 2017; pp. 1–5.
31. Liu, Y.; Liu, J.; Argyriou, A.; Ci, S. MEC-Assisted Panoramic VR Video Streaming over Millimeter Wave Mobile Networks. *IEEE Trans. Multimed.* **2019**, *21*, 1302–1316. [CrossRef]
32. Du, J.; Yu, F.R.; Lu, G.; Wang, J.; Jiang, J.; Chu, X. MEC-Assisted Immersive VR Video Streaming over Terahertz Wireless Networks: A Deep Reinforcement Learning Approach. *IEEE Internet Things J.* **2020**, *7*, 9517–9529. [CrossRef]
33. Liu, X.; Deng, Y. Learning-Based Prediction, Rendering and Association Optimization for MEC-Enabled Wireless Virtual Reality (VR) Networks. *IEEE Trans. Wirel. Commun.* **2021**, *20*, 6356–6370. [CrossRef]
34. Liu, Y.; Liu, J.; Argyriou, A.; Wang, L.; Xu, Z. Rendering-Aware VR Video Caching Over Multi-Cell MEC Networks. *IEEE Trans. Veh. Technol.* **2021**, *70*, 2728–2742. [CrossRef]
35. Dai, Y.; Zhang, Y. Adaptive Digital Twin for Vehicular Edge Computing and Networks. *J. Commun. Inf. Netw.* **2022**, *7*, 48–59.
36. Zhang, L.; Chakareski, J. UAV-Assisted Edge Computing and Streaming for Wireless Virtual Reality: Analysis, Algorithm Design, and Performance Guarantees. *IEEE Trans. Veh. Technol.* **2022**, *71*, 3267–3275. [CrossRef]
37. Zhong, L.; Chen, X.; Xu, C.; Ma, Y.; Wang, M.; Zhao, Y.; Muntean, G.M. A Multi-User Cost-Efficient Crowd-Assisted VR Content Delivery Solution in 5G-and-Beyond Heterogeneous Networks. *IEEE Trans. Mob. Comput.* 2022, *early access*. [CrossRef]
38. Le Callet, P.; Möller, S.; Perkis, A. (Eds.) *Qualinet White Paper on Definitions of Quality of Experience*; EU COST Action IC 1003 QUALINET: Lausanne, Switzerland, 2013.
39. Recommendation ITU-T P.10/G.100. *Vocabulary for Performance, Quality of Service and Quality of Experience*; International Telecommunication Union—Telecommunication Standardization Sector: Geneva, Switzerland, 2016.
40. Reiter, U.; Brunnström, K.; De Moor, K.; Larabi, M.-C.; Pereira, M.; Pinheiro, A.; You, J.; Zgank, A. Factors influencing quality of experience. In *Quality of Experience*; Möller, S., Raake, A., Eds.; T-Labs Series in Telecommunication Services; Springer: New York, NY, USA, 2014.
41. Zepernick, H.J.; Engelke, U. Quality of Experience of Multimedia Services: Past, Present, and Future. In Proceedings of the European Conference on Interactive TV and Video, Lisbon, Portugal, 29 June–1 July 2011; pp. 1–5.
42. Laghari, A.A.; He, H.; Khan, A.; Kumar, N.; Kharel, R. Quality of Experience Framework for Cloud Computing (QoC). *IEEE Access* **2018**, *6*, 64876–64889. [CrossRef]
43. Azevedo, R.G.D.A.; Birkbeck, N.; Simone, F.D.; Janatra, I.; Adsumilli, B.; Frossard, P. Visual Distortions in 360° Videos. *IEEE Trans. Circuits Syst. Video Technol.* **2020**, *30*, 2524–2537.
44. Chiariotti, F. A Survey on 360° Video: Coding, Quality of Experience and Streaming. *Comput. Commun.* **2021**, *177*, 133–155.
45. Hu, F.; Deng, Y.; Saad, W.; Bennis, M.; Aghvami, A.H. Cellular-Connected Wireless Virtual Reality: Requirements, Challenges, and Solutions. *IEEE Commun. Mag.* **2020**, *58*, 105–110. [CrossRef]
46. Müller, A.; Yang, H.C. Dual-Hop Adaptive Packet Transmission Systems with Regenerative Relaying. *IEEE Trans. Wirel. Commun.* **2010**, *9*, 234–244. [CrossRef]
47. Liu, Q.; Zhou, S.; Giannakis, G.B. Cross-Layer Combining of Adaptive Modulation and Coding with Truncated ARQ over Wireless Links. *IEEE Trans. Wirel. Commun.* **2004**, *3*, 1746–1755. [CrossRef]
48. Gradshteyn, I.S.; Ryzhik, I.M. *Table of Integrals, Series, and Products*, 7th ed.; Academic Press: Cambridge, MA, USA, 2007.
49. Bianchi, G. Performance Analysis of the IEEE 802.11 Distributed Coordination Function. *IEEE J. Sel. Areas Commun.* **2000**, *18*, 535–547. [CrossRef]
50. WirelessHD. *Overview of WirelessHD Specification Version 1.1*; Broadcom Co.: San Jose, CA, USA; Intel Co.: San Francisco, CA, USA; LG Electronics Inc.: Seoul, Korea; NEC Co.: Tokyo, Japan; Panasonic Co.: Osaka, Japan; Royal Philips Electronics: Amsterdam, The Netherlands; Samsung Electronics Co. LTD: Suwon, Korea; SiBEAM Inc.: Sunnyvale, CA, USA; Sony Co.: Tokyo, Japan; Toshiba Co.: Tokyo, Japan, 2010.
51. TPCAST. *TPCAST Business Edition*; TPCAST: Amsterdam, The Netherlands, 2017.
52. IEEE 802. *IEEE P802.11 Task Group BE (EHT) Meeting Update*. Available online: http://www.ieee802.org/11/Reports/tgbe_update.htm (accessed on 25 September 2021).